

# SU(3) Chiral Dynamics with Coupled Channels: Eta and Kaon Photoproduction

N. Kaiser, T. Waas and W. Weise

*Physik Department, Technische Universität München  
Institut für Theoretische Physik, D-85747 Garching, Germany*

## Abstract

We identify the leading s-wave amplitudes of the SU(3) chiral meson-baryon Lagrangian with an effective coupled-channel potential which is iterated in a Lippmann-Schwinger equation. The strangeness  $S = -1$  resonance  $\Lambda(1405)$  and the  $S_{11}(1535)$  nucleon resonance emerge as quasi-bound states of anti-kaon/nucleon and kaon/ $\Sigma$ -hyperon. Our approach to meson photoproduction introduces no new parameters. By adjusting a few finite range parameters we are able to simultaneously describe a large amount of low energy data. These include the cross sections of  $K^-p$  elastic and inelastic scattering, the cross sections of eta meson and kaon photoproduction from nucleons as well as those of pion induced production of etas and kaons (16 different reaction channels altogether).

arXiv:hep-ph/9607459v1 29 Jul 1996

\*Work supported in part by BMBF and GSI

## I. INTRODUCTION

Over the last few years there has been renewed interest in the photoproduction of eta mesons and kaons from nucleons. At MAMI (Mainz) very precise differential cross sections for the reaction  $\gamma p \rightarrow \eta p$  have been measured from threshold at 707 MeV up to 800 MeV photon lab energy [1]. The nearly isotropic angular distributions show a clear dominance of the s-wave amplitude (electric dipole) in this energy range. At ELSA (Bonn) an analogous  $\eta$ -electroproduction experiment has been performed [2] at higher beam energies but with very low virtual photon momentum transfer,  $q^2 = -0.056 \text{ GeV}^2$ , thus the combined data cover the whole energy range of the nucleon resonance  $S_{11}(1535)$ . The latter has the outstanding feature of a strong  $\eta N$  decay [3] which is made responsible for the observed large cross sections. Recently the incoherent  $\eta$ -photoproduction from the deuteron has also been measured at MAMI [4] which allows for a preliminary extraction of the  $\gamma n \rightarrow \eta n$  cross sections [5]. Upcoming coincidence measurements of the  $\eta$ -meson together with a recoiling nucleon will reduce the present uncertainties coming from the deuteron structure. At ELSA there is an ongoing program to measure strangeness production with photons from proton targets. Cross sections for the reactions  $\gamma p \rightarrow K^+ \Lambda$  and  $\gamma p \rightarrow K^+ \Sigma^0$  have been measured with improved accuracy from the respective thresholds at 911 and 1046 MeV photon lab energy up to 1.5 GeV together with angular distributions and recoil hyperon polarizations [6]. The analysis of the neutral kaon channel  $\gamma p \rightarrow K^0 \Sigma^+$  (considering the same energy range and observables) is presently performed [7] and will lead to a substantial improvement of the data base. The ultimate aim of these experimental investigations is a complete multipole analysis in the low energy region and in particular a determination of the s-wave multipole,  $E_{0+}$ , (i.e. the electric dipole amplitude) close to threshold. The knowledge of these multipoles will permit crucial tests of models for strangeness production.

Most theoretical models used to describe the abovementioned reactions are based on an effective Lagrangian approach including Born terms and various (meson and baryon) resonance exchanges [8–13] with the coupling constants partly fixed by independent electromagnetic and hadronic data. In the work of [10] it was furthermore tried to extract the  $\eta NN$  coupling constant from a best fit to the data and to decide whether the  $\eta NN$  vertex is of pseudoscalar or pseudovector nature. Ref. [13] used a K-matrix model with parameters adjusted to  $S_{11}$  partial wave (orbital angular momentum  $l = 0$ , total isospin  $I = 1/2$ ) of  $\pi N$  scattering and predicted quite successfully the cross sections for pion induced  $\eta$ -production  $\pi^- p \rightarrow \eta n$ . The  $\eta$ -photoproduction involves as new parameters the photoexcitation strengths of two  $S_{11}$ -resonances which are furthermore constrained by pion photoproduction in the considered energy range. Ref. [13] finds a good description of the MAMI data whereas the ELSA data above the resonance peak are somewhat underestimated. Whereas resonance models work well for  $\eta$ -production the situation is more difficult for kaon production where several different kaon-hyperon final states are possible. As shown in [11] resonance models lead to a notorious overprediction of the  $\gamma p \rightarrow K^0 \Sigma^+$  and  $\gamma n \rightarrow K^+ \Sigma^-$  cross section. Only a drastic reduction of the  $K \Sigma N$  coupling constant to nearly a tenth of its SU(3) value gives a reasonable fit to all available data. This is clearly not a convincing solution to the problem.

We will use here quite a different approach to eta and kaon photoproduction (and the related pion induced reactions) not introducing any explicit resonance. Our starting point is the SU(3) chiral effective meson-baryon Lagrangian at next-to-leading order, the low

energy effective field theory which respects the symmetries of QCD (in particular chiral symmetry). The explicit degrees of freedom are only the baryon and pseudoscalar meson octet with interactions controlled by chiral symmetry and a low energy expansion. As shown in previous work [14,15] the effective Lagrangian predicts a strong attraction in certain channels such as the  $\overline{K}N$  isospin  $I = 0$  and the  $K\Sigma$  isospin  $I = 1/2$  s-waves. If this attraction is iterated to infinite orders in a potential approach (not performing the systematic loop expansion of chiral perturbation theory) one can dynamically generate the  $\Lambda(1405)$  and the  $S_{11}(1535)$  as quasi-bound meson-baryon states with all properties attributed to these resonances. The purpose of this paper is to extend the coupled channel potential approach to meson photo and electroproduction. To the order we are working this extension does not introduce any further parameter compared to the pure strong interaction case. It is then quite non-trivial to find a good description of so many available photon and pion induced data for this multi-channel problem with just a few free parameters. For both the strong meson-baryon scattering and the meson photoproduction processes we will consider only s-waves in this work. Therefore the comparison with data is necessarily restricted to the near threshold region. The s-wave approximation excludes the calculation of observables like recoil polarization which arises from s- and p-wave interference terms. The systematic inclusion of p-waves goes beyond the scope of this paper and will be considered in the future.

The paper is organized as follows. In the second section we describe the effective  $SU(3)$  chiral meson-baryon Lagrangian at next-to-leading order and we present the potential model to calculate strong meson-baryon scattering and meson photoproduction simultaneously. In the third section we discuss our results, the low energy cross sections for the six channels present in  $K^-$ -proton scattering,  $K^-p \rightarrow K^-p$ ,  $\overline{K}^0n$ ,  $\pi^0\Lambda$ ,  $\pi^+\Sigma^-$ ,  $\pi^0\Sigma^0$ ,  $\pi^-\Sigma^+$ , the cross sections of eta and kaon photoproduction from protons (and neutrons)  $\gamma p \rightarrow \eta p$ ,  $K^+\Lambda$ ,  $K^+\Sigma^0$ ,  $K^0\Sigma^+$  and  $\gamma n \rightarrow \eta n$ , as well as those of the corresponding pion induced reactions  $\pi^-p \rightarrow \eta n$ ,  $K^0\Lambda$ ,  $K^0\Sigma^0$ ,  $K^+\Sigma^-$  and  $\pi^+p \rightarrow K^+\Sigma^+$ . We furthermore make a prediction for the longitudinal to transverse ratio in  $\eta$ -electroproduction and discuss the nature of the  $S_{11}(1535)$ -resonance in our approach. In the appendix we collect some lengthy formulae.

## II. FORMALISM

### A. Effective Chiral Lagrangian

The tool to investigate the dynamical implications of spontaneous and explicit chiral symmetry breaking in QCD is the effective chiral Lagrangian. It provides a non-linear realization of the chiral symmetry group  $SU(3)_L \times SU(3)_R$  in terms of the effective low energy degrees of freedom, which are the pseudoscalar Goldstone bosons ( $\pi$ ,  $K$ ,  $\eta$ ) and the octet baryons ( $N$ ,  $\Lambda$ ,  $\Sigma$ ,  $\Xi$ ). The effective Lagrangian can be written generally as [16]

$$\mathcal{L} = \mathcal{L}_{\phi B}^{(1)} + \mathcal{L}_{\phi B}^{(2)} + \dots \quad (1)$$

corresponding to an expansion in increasing number of derivatives (external momenta) and quark masses. In the relativistic formalism the leading order term reads

$$\mathcal{L}_{\phi B}^{(1)} = \text{tr}(\overline{B}(i\gamma_\mu D^\mu - M_0)B) + F \text{tr}(\overline{B}\gamma_\mu\gamma_5[w^\mu, B]) + D \text{tr}(\overline{B}\gamma_\mu\gamma_5\{w^\mu, B\}) \quad (2)$$

where

$$D^\mu B = \partial^\mu B - ie[Q, B]A^\mu + \frac{1}{8f^2}[[\phi, \partial^\mu \phi], B] + \dots \quad (3)$$

is the chiral covariant derivative and

$$w^\mu = -\frac{1}{2f}\partial^\mu \phi + \frac{ie}{2f}[Q, \phi]A^\mu + \dots \quad (4)$$

is an axial vector quantity. The  $SU(3)$  matrices  $\phi$  and  $B$  collect the octet pseudoscalar meson fields and the octet baryon fields, respectively. For later use the photon field  $A^\mu$  has been included via minimal substitution with  $Q = \frac{1}{3}\text{diag}(2, -1, -1)$  the quark charge operator. The scale parameter  $f$  is the pseudoscalar meson decay constant (in the chiral limit) which we identify throughout with the pion decay constant  $f = 92.4$  MeV.  $F \simeq 0.5$  and  $D \simeq 0.8$  are the  $SU(3)$  axial vector coupling constants subject to the constraint  $D + F = g_A = 1.26$ . The mass  $M_0$  is the common octet baryon mass in the chiral limit, which we identify with an average octet mass.

At next-to-leading order the terms relevant for s-wave scattering are

$$\begin{aligned} \mathcal{L}_{\phi B}^{(2)} = & b_D \text{tr}(\overline{B}\{\chi_+, B\}) + b_F \text{tr}(\overline{B}[\chi_+, B]) + b_0 \text{tr}(\overline{B}B) \text{tr}(\chi_+) \\ & + 2d_D \text{tr}(\overline{B}\{(v \cdot u)^2, B\}) + 2d_F \text{tr}(\overline{B}[(v \cdot u)^2, B]) \\ & + 2d_0 \text{tr}(\overline{B}B) \text{tr}((v \cdot u)^2) + 2d_1 \text{tr}(\overline{B}v \cdot u) \text{tr}(v \cdot uB) \end{aligned} \quad (5)$$

with

$$\chi_+ = 2\chi_0 - \frac{1}{4f^2}\{\phi, \{\phi, \chi_0\}\} + \dots, \quad \chi_0 = \text{diag}(m_\pi^2, m_\pi^2, 2m_K^2 - m_\pi^2). \quad (6)$$

The first three terms in eq.(5) are chiral symmetry breaking terms linear in the quark masses. Using the Gell-Mann-Oakes-Renner relation for the Goldstone boson masses these can be expressed through  $m_\pi^2$  and  $m_K^2$  as done in eq.(6). Two of the three parameters  $b_D, b_F, b_0$  can be fixed from the mass splittings in the baryon octet

$$\begin{aligned} M_\Sigma - M_\Lambda &= \frac{16}{3}b_D(m_K^2 - m_\pi^2), \quad M_\Xi - M_N = 8b_F(m_\pi^2 - m_K^2), \\ M_\Sigma - M_N &= 4(b_D - b_F)(m_K^2 - m_\pi^2). \end{aligned} \quad (7)$$

In a best fit to the isospin averaged baryon masses using the charged meson masses one finds the values  $b_D = +0.066$  GeV<sup>-1</sup> and  $b_F = -0.213$  GeV<sup>-1</sup>. The  $b_0$ -term shifts the whole baryon octet by the same amount, so one needs a further piece of information to fix  $b_0$ , which is the pion-nucleon sigma term (empirical value  $45 \pm 8$  MeV [17])

$$\sigma_{\pi N} = \langle N | \hat{m}(\bar{u}u + \bar{d}d) | N \rangle = -2m_\pi^2(b_D + b_F + 2b_0) \quad (8)$$

with  $\hat{m} = (m_u + m_d)/2$  the average light quark mass. At the same time the strangeness content of the proton is given by

$$y = \frac{2\langle p | \bar{s}s | p \rangle}{\langle p | \bar{u}u + \bar{d}d | p \rangle} = \frac{2(b_0 + b_D - b_F)}{2b_0 + b_D + b_F} \quad (9)$$

whose "empirical" value is presently  $y = 0.2 \pm 0.2$  [17]. If one stays to linear order in the quark masses, as done here, then both pieces of information ( $\sigma_{\pi N}$  and  $y$ ) can not be explained by a single value of  $b_0$ . We will later actually fit  $b_0$  to many scattering data within the bounds,  $-0.52 \text{ GeV}^{-1} < b_0 < -0.28 \text{ GeV}^{-1}$  set by the empirical  $\sigma_{\pi N}$  and  $y$ . The experimentally unknown kaon-proton sigma term

$$\sigma_{Kp} = \frac{1}{2}(\hat{m} + m_s)\langle p|\bar{u}u + \bar{s}s|p\rangle = -4m_K^2(b_D + b_0) \quad (10)$$

can then be estimated to linear order in the quark mass.

The last two lines in eq.(5) comprise the general set of order  $q^2$  terms contributing to s-wave meson-baryon scattering. They are written in the heavy baryon language with  $v^\mu$  a four-velocity which allows to select a frame of reference (in our case the meson-baryon center of mass frame). Note that in comparison to previous work [14,15] we use here the minimal set of linearly independent terms. The additional term  $d_2 \text{tr}(\bar{B}v \cdot u B v \cdot u)$  can be expressed through the ones given in eq.(5) using some trace identities of  $SU(3)$ . Of course the physical content remains the same if one works with an overcomplete basis as done in [14,15]. The parameters  $d_D, d_F, d_0, d_1$  are not known a priori, but instead of fitting all of them from data we put two constraints on them,

$$4\pi\left(1 + \frac{m_\pi}{M_N}\right)a_{\pi N}^+ = \frac{m_\pi^2}{f^2}\left(d_D + d_F + 2d_0 - 4b_0 - 2b_F - 2b_D - \frac{g_A^2}{4M_N}\right) + \frac{3g_A^2 m_\pi^3}{64\pi f^4} \quad (11)$$

and

$$4\pi\left(1 + \frac{m_K}{M_N}\right)a_{KN}^0 = \frac{m_K^2}{f^2}\left(4b_F - 4b_0 - 2d_F + 2d_0 - d_1 + \frac{D}{M_N}\left(F - \frac{D}{3}\right)\right). \quad (12)$$

Here  $a_{\pi N}^+$  is the isospin-even  $\pi N$  s-wave scattering length and  $a_{KN}^0$  the isospin zero kaon-nucleon s-wave scattering length which are both very small ( $a_{\pi N}^+ = (-0.012 \pm 0.06) \text{ fm}$  [18],  $a_{KN}^0 = -0.1 \pm 0.1 \text{ fm}$  [19]). The expression for  $a_{\pi N}^+$  includes the non-analytic loop correction proportional to  $m_\pi^3$  calculated in [20], and we have corrected sign misprints in the formula for  $a_{KN}^0$  occurring in [14]. In essence the relations eqs.(11,12) imply that these linear combinations of  $b$ - and  $d$ -parameters are an order of magnitude smaller than the individual entries. This completes the description of the  $SU(3)$  chiral meson-baryon Lagrangian at next-to-leading order and we conclude that there are only two combinations of  $d$ -parameters left free. These will be fixed in a fit to many scattering data.

## B. Coupled Channel Approach

Whereas the systematic approach to chiral dynamics is chiral perturbation theory, a renormalized perturbative loop-expansion, its range of applicability can be very small in cases where strong resonances lie closely above (or even slightly below) the reaction threshold. Prominent examples for this are the isospin  $I = 0$ , strangeness  $S = -1$  resonance  $\Lambda(1405)$  in  $K^-$ -proton scattering, or the  $S_{11}(1535)$  nucleon resonance which has an outstandingly large coupling to the  $\eta N$ -channel and therefore is an essential ingredient in the description of  $\eta$ -photoproduction. In previous work [14,15] we have shown that the chiral effective Lagrangian is a good starting point to dynamically generate such resonances. The chiral Lagrangian predicts strongly attractive forces in the  $\bar{K}N$  isospin

0 and  $K\Sigma$  isospin 1/2 channels. If this strong attraction is iterated to all orders, e.g. via a Lippmann-Schwinger equation in momentum space or a local coordinate-space potential description, quasi-bound meson-baryon states emerge which indeed have all the characteristic properties of the  $\Lambda(1405)$  or the  $S_{11}(1535)$  (e.g. the  $K\Sigma$  isospin 1/2 quasi-bound state has a large branching ratio for decaying into  $\eta N$ ). The price to be paid in this approach are some additional finite range parameters, which must be fitted to data. However, since we are dealing with a multi-channel problem, it is quite non-trivial to find a satisfactory description of the data in all reaction channels with so few free parameters.

Let us now describe the potential approach to meson-baryon scattering developed in [14,15] and show how it can be generalized to meson photoproduction. The indices  $i$  and  $j$  label the meson-baryon channels involved. They are coupled through a potential in momentum space

$$V_{ij} = \frac{\sqrt{M_i M_j}}{4\pi f^2 \sqrt{s}} C_{ij} , \quad (13)$$

where the relative coupling strengths  $C_{ij}$  are, up to a factor  $-f^{-2}$ , the corresponding s-wave amplitudes calculated from the  $SU(3)$  chiral meson-baryon Lagrangian eqs.(2,5) to order  $q^2$ , which means at most quadratic in the meson center of mass energy

$$E_i = \frac{s - M_i^2 + m_i^2}{2\sqrt{s}} \quad (14)$$

and the meson mass. Here  $\sqrt{s}$  is the total center of mass energy and  $M_i$  and  $m_i$  stand for the masses of the baryon and meson in channel  $i$ , respectively. The potential  $V_{ij}$  is iterated to all orders in a Lippmann-Schwinger equation of the form

$$T_{ij} = V_{ij} + \sum_n \frac{2}{\pi} \int_0^\infty dl \frac{l^2}{k_n^2 + i0 - l^2} \left( \frac{\alpha_n^2 + k_n^2}{\alpha_n^2 + l^2} \right)^2 V_{in} T_{nj} , \quad (15)$$

with  $T_{ij}$  the resulting  $T$ -matrix connecting the in- and outgoing channels  $j$  and  $i$ . In eq.(15) the index  $n$  labels the intermediate meson-baryon states to be summed over and  $\vec{l}$  is the relative momentum of the off-shell meson-baryon pair in intermediate channel  $n$ . The propagator used in eq.(15) is proportional to a (simple) non-relativistic energy denominator with  $k_n = \sqrt{E_n^2 - m_n^2}$  the on-shell relative momentum. The potentials derived from the chiral Lagrangian have zero range since they stem from a contact interaction. To make the  $dl$ -integration convergent a form factor parametrizing finite range aspects of the potential has to be introduced. This is done via a dipole-like off-shell form factor  $[(\alpha_n^2 + k_n^2)/(\alpha_n^2 + l^2)]^2$  in eq.(15) with  $\alpha_n$  a finite range parameter for each channel  $n$ . The form chosen here has the property that on-shell, i.e. for  $l = k_n$ , it becomes identical to one. From physical considerations one expects the cut-offs  $\alpha_n$  to lie in the range 0.3 GeV to 1 GeV reminiscent of the scales related to two-pion exchange or vector meson exchange. We will actually fix the cut-offs  $\alpha_n$  in a fit to many data keeping in mind physically reasonable ranges. We note that other than dipole form of the off-shell form factor in eq.(15) have led to similarly good results. The Lippmann-Schwinger equation for the multi-channel  $T$ -matrix  $T_{ij}$  can be solved in closed form by simple matrix inversion

$$T = (1 - V \cdot G)^{-1} \cdot V , \quad (16)$$

where  $G$  is the diagonal matrix with entries

$$G_n = \frac{k_n^2}{2\alpha_n} - \frac{\alpha_n}{2} - i k_n , \quad (17)$$

with  $k_n = \sqrt{E_n^2 - m_n^2}$  and the appropriate analytic continuation ( $i|k_n|$  below threshold  $E_n < m_n$ ). The resulting  $S$ -matrix

$$S_{ij} = \delta_{ij} - 2i\sqrt{k_i k_j} T_{ij} \quad (18)$$

is exactly unitary in the subspace of the (kinematically) open channels (but not crossing symmetric) and the total (s-wave) cross section for the reaction ( $j \rightarrow i$ ) is calculated via

$$\sigma_{ij} = 4\pi \frac{k_i}{k_j} |T_{ij}|^2 . \quad (19)$$

We note that the kinematical prefactor in eq.(13) has been chosen such that in Born approximation, i.e.  $T_{ij} = V_{ij}$ , the cross section  $\sigma_{ij}$  has the proper relativistic flux factor. Furthermore, one can see that the imaginary part of the Born series eq.(16) truncated at quadratic order in the potential matrix  $V$  agrees with the one of a one-loop calculation in chiral perturbation theory. This is so because  $M_n k_n / 4\pi\sqrt{s}$  is the invariant two-particle phase space and the chosen off-shell form factor is unity on-shell. However, the real parts do not show chiral logarithms which would result from a proper evaluation of four-dimensional loop integrals.

This concludes the general description of our coupled channel approach. We will first apply it to the six channel problem of  $K^-p$  scattering (involving the channels  $\pi^+\Sigma^-, \pi^0\Sigma^0, \pi^-\Sigma^+, \pi^0\Lambda, K^-p, \overline{K^0}n$ ). The corresponding potential strengths  $C_{ij}$  can be found in appendix B of [14], setting  $d_2 = 0$ . Secondly we use it for the four-channel system of  $\pi N, \eta N, K\Lambda, K\Sigma$  states with total isospin 1/2 and the two channel system of  $\pi N, K\Sigma$  states with total isospin 3/2, with the corresponding  $C_{ij}$  given in the appendix.

### C. Meson Photo- and Electroproduction

We now extend the same formalism to s-wave meson photoproduction. As in [21] our basic assumption is that the s-wave photoproduction process can be described by a Lippmann-Schwinger equation. In complete analogy to our description of the strong interaction we will identify the s-wave photoproduction potential (named  $B_{0+}$ ) with the electric dipole amplitude  $E_{0+}$  calculated to order  $q^2$  from the chiral effective Lagrangian. A welcome feature of such an approach is that it does not introduce any further adjustable parameter. Consequently meson-baryon interactions and meson photoproduction are strongly tied together and the fits of e.g. the finite range parameters are controlled by both sets of data. For the description of the photoproduction reactions  $\gamma p \rightarrow \eta p, K^+\Lambda, K^+\Sigma^0, K^0\Sigma^+$  we have to know the photoproduction potentials  $B_{0+}$  for  $\gamma p \rightarrow \phi B$ , where  $\phi B$  refers to the meson-baryon states with total isospin  $I = 1/2$  or  $I = 3/2$  and isospin projection  $I_3 = +1/2$ . We label these states by an index which runs from 1 to 6, which refers to  $|\pi N\rangle^{(1/2)}, |\eta N\rangle^{(1/2)}, |K\Lambda\rangle^{(1/2)}, |K\Sigma\rangle^{(1/2)}, |\pi N\rangle^{(3/2)}$  and  $|K\Sigma\rangle^{(3/2)}$ , in that order. The resulting expressions involve as parameters only the axial vector coupling constants  $F$  and  $D$  and read

$$\begin{aligned}
B_{0+}^{(1)} &= \frac{eM_N}{8\pi f\sqrt{3s}}(D+F)(2X_\pi + Y_\pi) , \\
B_{0+}^{(2)} &= \frac{eM_N}{8\pi f\sqrt{3s}}(3F-D)Y_\eta , \\
B_{0+}^{(3)} &= \frac{e\sqrt{M_N M_\Lambda}}{8\pi f\sqrt{3s}}(-D-3F)X_K , \\
B_{0+}^{(4)} &= \frac{e\sqrt{M_N M_\Sigma}}{8\pi f\sqrt{3s}}(D-F)(X_K + 2Y_K) , \\
B_{0+}^{(5)} &= \frac{e\sqrt{2}M_N}{8\pi f\sqrt{3s}}(D+F)(Y_\pi - X_\pi) , \\
B_{0+}^{(6)} &= \frac{e\sqrt{2M_N M_\Sigma}}{8\pi f\sqrt{3s}}(D-F)(X_K - Y_K) , \tag{20}
\end{aligned}$$

where  $X_\phi$  and  $Y_\phi$  are dimensionless functions depending on the center of mass energy  $E_\phi$  and the mass  $m_\phi$  of the photoproduced meson.  $X_\phi$  takes the form

$$X_\phi = \frac{1}{2} - \frac{1}{4M_0} \left( 2E_\phi + \frac{m_\phi^2}{E_\phi} \right) + \left( 1 + \frac{m_\phi^2}{2M_0 E_\phi} \right) \frac{m_\phi^2}{2E_\phi \sqrt{E_\phi^2 - m_\phi^2}} \ln \frac{E_\phi + \sqrt{E_\phi^2 - m_\phi^2}}{m_\phi} , \tag{21}$$

and it sums up the contributions of all tree diagrams to the s-wave photoproduction multipole of a positively charged meson. The logarithmic term comes from the meson pole diagram in which the photon couples to the positively charged meson, and its analytic continuation below threshold ( $E_\phi < m_\phi$ ) is done via the formula

$$\frac{\ln(x + \sqrt{x^2 - 1})}{\sqrt{x^2 - 1}} = \frac{\arccos x}{\sqrt{1 - x^2}} . \tag{22}$$

If the photoproduced meson is neutral the corresponding sum of diagrams leads to a simpler expression,

$$Y_\phi = -\frac{1}{3M_0} \left( 2E_\phi + \frac{m_\phi^2}{E_\phi} \right) , \tag{23}$$

for the reduced s-wave multipole. Infinitely many rescatterings of the photoproduced meson-baryon state due to the strong interaction are summed up via the Lippmann-Schwinger equation. This is shown graphically in Fig.1. The "full" electric dipole amplitude  $E_{0+}^{(i)}$  for channel  $i$  is then given by

$$E_{0+}^{(i)} = \sum_j [(1 - V \cdot G)^{-1}]_{ij} B_{0+}^{(j)} , \tag{24}$$

where  $V$  is the matrix of the strong interaction potential and  $G$  the diagonal propagator matrix defined in eq.(17). We note that the "full"  $E_{0+}$  amplitudes fulfill Watson's final state theorem, i.e. the phase of the complex number  $E_{0+}$  is equal to the strong interaction phase (in this simple form the theorem applies only below the  $\eta N$  threshold where just one channel is open). From  $E_{0+}^{(i)}$  one can finally compute the total (s-wave) photoproduction cross section for the meson-baryon final state  $i$ ,



$$\sigma_{\text{tot}}^{(i)} = 4\pi \frac{k_i}{k_\gamma} |E_{0+}^{(i)}|^2, \quad (25)$$

with  $k_\gamma = (s - M_N^2)/2\sqrt{s}$  the photon center of mass energy and  $s = M_N^2 + 2M_N E_\gamma^{\text{lab}}$  in terms of the photon lab energy  $E_\gamma^{\text{lab}}$ .

We also calculate within the present framework the cross section for  $\eta$ -photoproduction from neutrons ( $\gamma n \rightarrow \eta n$ ). For this purpose we have to know the photoproduction potentials for  $\gamma n \rightarrow \phi B$ , where  $\phi B$  is a meson-baryon state with total isospin  $I = 1/2$  and third component  $I_3 = -1/2$ . The respective potentials are distinguished by a tilde from the previous ones and read

$$\begin{aligned} \tilde{B}_{0+}^{(1)} &= \frac{eM_N}{4\pi f\sqrt{3s}}(D + F)(Y_\pi - X_\pi), \\ \tilde{B}_{0+}^{(2)} &= \tilde{B}_{0+}^{(3)} = 0, \\ \tilde{B}_{0+}^{(4)} &= \frac{e\sqrt{M_N M_\Sigma}}{4\pi f\sqrt{3s}}(D - F)(X_K - Y_K). \end{aligned} \quad (26)$$

The reason for the second ( $\gamma n \rightarrow \eta n$ ) and third ( $\gamma n \rightarrow K^0 \Lambda$ ) neutron photoproduction potential being zero is that here the final state involves a neutral baryon and a neutral meson to which the photon cannot couple directly (via the charge). Thus the s-wave meson photoproduction amplitude vanishes to order  $q^2$  in these channels. We will see later that the  $K\Lambda$  channel is very important for  $\eta$ -production off the proton and therefore the order  $q^2$  result  $\tilde{B}_{0+}^{(3)} = 0$  will lead to a too strong reduction of the  $\gamma n \rightarrow \eta n$  cross section. To cure this problem, we include for these double neutral channels ( $\eta n, K^0 \Lambda$ ) the first correction arising from the coupling of the photon to the neutral baryon via the anomalous magnetic moment

$$\begin{aligned} \delta\tilde{B}_{0+}^{(2)} &= \frac{eM_N \kappa_n}{48\pi f M_0^2 \sqrt{3s}}(3F - D)(4E_\eta^2 - m_\eta^2), \\ \delta\tilde{B}_{0+}^{(3)} &= \frac{e\sqrt{M_N M_\Lambda}}{96\pi f M_0^2 \sqrt{3s}}(D + 3F)[\kappa_\Lambda(2m_K^2 - 5E_K^2) - 3\kappa_n E_K^2], \end{aligned} \quad (27)$$

where  $\kappa_n = -1.913$  and  $\kappa_\Lambda = -0.613$  are the anomalous magnetic moments of the neutron and the  $\Lambda$ -hyperon.

The extension of our formalism to meson electroproduction (in s-waves) is straightforward. In electroproduction one has to consider two s-wave multipoles, the transverse one  $E_{0+}$  and the longitudinal one  $L_{0+}$ , which furthermore depend on the virtual photon momentum transfer  $q^2 < 0$ . All steps previously mentioned to construct the s-wave multipole  $E_{0+}$  apply to the longitudinal  $L_{0+}$  as well. One only has to generalize the functions  $X_\phi$  and  $Y_\phi$  to a transverse and a longitudinal version, which furthermore depend on the virtual photon momentum transfer  $q^2 < 0$ . The corresponding somewhat lengthy formulae for  $X_\phi^{\text{trans}}$  and  $X_\phi^{\text{long}}$  can be found in the appendix whereas the  $Y_\phi$ -functions do not change,  $Y_\phi^{\text{trans}} = Y_\phi^{\text{long}} = Y_\phi$ , with  $Y_\phi$  given in eq.(23). This completes the discussion of the formalism necessary to describe meson photo- and electroproduction within our coupled channel approach.

### III. RESULTS

First we have to fix the parameters. For the six channels involved in  $K^-p$  scattering we work, as in [14], in the particle basis taking into account isospin breaking in the baryon and meson masses but use potentials  $C_{ij}$  calculated in the isospin limit. Then the  $K^-p$  and  $\overline{K^0}n$  threshold are split and cusps at the  $\overline{K^0}n$  threshold become visible in the cross sections. In this six channel problem we allow for three adjustable range parameters  $\alpha_{\overline{K}N}$ ,  $\alpha_{\pi\Lambda}$  and  $\alpha_{\pi\Sigma}$ . For the coupled  $(\pi N, \eta N, K\Lambda, K\Sigma)$  system we work in the isospin basis as mentioned in section II.B and use masses  $m_\pi = 139.57$  MeV,  $m_K = 493.65$  MeV,  $m_\eta = 547.45$  MeV,  $M_N = 938.27$  MeV,  $M_\Lambda = 1115.63$  MeV and  $M_\Sigma = 1192.55$  MeV, a choice which averages out most isospin breaking effects. Here we allow for four adjustable range parameters  $\alpha_{\pi N}$ ,  $\alpha_{\eta N}$ ,  $\alpha_{K\Lambda}$  and  $\alpha_{K\Sigma}$ . These seven range parameters and the two unconstrained combinations of  $d$ -parameters (in the chiral Lagrangian) were fixed in a best fit to the data discussed below. We also allowed for optimizing the parameters  $M_0$ ,  $b_0$  and  $D$  within narrow ranges. The best fit gave for the latter  $D = 0.782$ ,  $M_0 = 1054$  MeV and  $b_0 = -0.3036$  GeV $^{-1}$ . The last number, together with the known  $b_D, b_F$  leads to

$$\sigma_{\pi N} = 29.4 \text{ MeV}, \quad y = 0.065, \quad \sigma_{Kp} = 231.6 \text{ MeV} \quad (28)$$

Clearly, as expected the  $\pi N$ -sigma term is too small if  $y$  (the strangeness content of the proton is small) and the  $Kp$ -sigma term is in reasonable agreement with other estimates. For the other Lagrangian parameters we find  $d_0 = -0.9189$  GeV $^{-1}$ ,  $d_D = 0.3351$  GeV $^{-1}$ ,  $d_F = -0.4004$  GeV $^{-1}$ ,  $d_1 = -0.0094$  GeV $^{-1}$ , subject to the two constraints eqs.(11,12). Note that these numbers are not directly comparable to those in [14,15], since here the linear dependent  $d_2$ -term has been eliminated. Instead one has to compare with  $d_0 + d_2/2$ ,  $d_D - d_2$ ,  $d_F$ ,  $d_1 + d_2$ . The best fit of the range parameters gives  $\alpha_{\overline{K}N} = 724$  MeV,  $\alpha_{\pi\Lambda} = 1131$  MeV,  $\alpha_{\pi\Sigma} = 200$  MeV and  $\alpha_{\pi N} = 522$  MeV,  $\alpha_{\eta N} = 665$  MeV,  $\alpha_{K\Lambda} = 1493$  MeV,  $\alpha_{K\Sigma} = 892$  MeV. (We give sufficiently many digits here in order to make the numerical results reproducible). One sees that most of the range parameters are indeed in the physically expected two-pion to vector meson mass range. We also note that the best fit is very rigid and does not allow e.g. for a 5% deviation of the parameters from the values quoted above. Let us now discuss the fits to the data in detail.

#### A. $K^-p$ Scattering

Fig.2 shows the results for the six  $K^-p$  elastic and inelastic channels  $K^-p \rightarrow K^-p$ ,  $\overline{K^0}n$ ,  $\pi^0\Lambda$ ,  $\pi^+\Sigma^-$ ,  $\pi^0\Sigma^0$ ,  $\pi^-\Sigma^+$ . As in [14] one finds good agreement with the available low energy data below 200 MeV kaon lab momentum. We present these results here just to make sure again that indeed a large amount of data can be fitted simultaneously. For the threshold branching ratios  $\gamma, R_c, R_n$  (defined in eq.(21) of [14]), we find here  $\gamma = 2.33$  ( $2.36 \pm 0.04$ ),  $R_c = 0.65$  ( $0.66 \pm 0.01$ ),  $R_n = -0.23$  ( $0.19 \pm 0.02$ ), where the numbers given in brackets are the empirical values. In Fig.2 one observes cusps in the cross sections at the  $\overline{K^0}n$  threshold, which are a consequence of unitarity and the opening of a new channel. Unfortunately the existing data are not precise enough to confirm this structure. The status of the  $K^-p$  scattering data will improve with DAΦNE at Frascati producing intense kaon beams at 127 MeV lab momentum, and in particular once the planned kaon facility at KEK will become available. Fig.3 shows real and imaginary

parts of the calculated total isospin  $I = 0$   $\bar{K}N$  s-wave scattering amplitude in the region  $1.35 \text{ GeV} < \sqrt{s} < 1.45 \text{ GeV}$ . The resonance structure around 1405 MeV is clearly visible. In our framework it is due to the formation of a quasi-bound  $\bar{K}N$ -state. It can decay into  $\pi\Sigma$  and thus receives its width of about 25 MeV. We want to stress here that no effort has been made to prescribe the position or width of the  $\Lambda(1405)$  below the  $K^-p$  threshold. Fig.3 results by merely fitting the scattering data in Fig.1 above the  $K^-p$  threshold (together with many other data).

## B. Eta and Kaon Photoproduction

The most precise data available are those for  $\eta$ -photoproduction off protons ( $\gamma p \rightarrow \eta p$ ) taken at MAMI [1] from threshold at 707 up to 800 MeV photon lab energy. These 54 data points of the total cross section (full circles) have the highest statistical weight in our fit and they can indeed be perfectly reproduced as seen in Fig.4. Note that the measured angular distribution of the  $\gamma p \rightarrow \eta p$  differential cross section [1] are almost isotropic, thus one can safely identify the total cross section with the s-wave cross section. For the ELSA data [2] (open squares) from 800 to 900 MeV photon lab energy one also finds very good agreement. Angular distributions have not been published for this case, so we assume s-wave dominance. Note that the ELSA data stem from electroproduction with a very low virtual photon momentum transfer of  $q^2 = -0.056 \text{ GeV}^2$ . We have actually checked that the corrections from the nonzero  $q^2$  and the longitudinal s-wave  $L_{0+}$  to the total cross section

$$\sigma_{\text{tot}} = 4\pi \frac{k_\eta}{k_\gamma} (|E_{0+}|^2 + \epsilon_L |L_{0+}|^2) \quad (29)$$

with  $\epsilon_L = -4\epsilon s q^2 (s - M_N^2 + q^2)^{-2}$  and  $\epsilon = 0.78$  (virtual photon polarization at the ELSA-experiment) are negligible (less than 6%) within error bars. For the s-wave multipole at the  $\eta p$  threshold we get

$$E_{0+}^{\text{thr}}(\gamma p \rightarrow \eta p) = (7.62 + 14.12i) \cdot 10^{-3} m_\pi^{-1} . \quad (30)$$

This number decomposes as follows. The potentials  $B_{0+}^{(j)}$  have the values 3.65,  $-2.25$ ,  $-15.97$  and  $0.78$  (in units of  $10^{-3} m_\pi^{-1}$ ) for the  $\pi N$ ,  $\eta N$ ,  $K\Lambda$ ,  $K\Sigma$  channels, respectively. The strong interaction part given by the matrix elements  $[(1 - V \cdot G)^{-1}]_{2j}$  in eq.(24) multiply these values by complex numbers  $(-0.48 + 0.54i)$ ,  $(1.35 + 0.39i)$ ,  $(-0.81 - 0.82i)$  and  $(-0.71 - 0.08i)$ , respectively. Interestingly, it is the initial photoexcitation of the  $K^+\Lambda$  state which after infinitely many rescatterings to  $\eta p$  makes the largest contribution. The absolute value  $|E_{0+}^{\text{thr}}| = 16.04 \cdot 10^{-3} m_\pi^{-1}$  is in good agreement with determinations in models having an explicit  $S_{11}(1535)$  resonance. Our ratio of imaginary part to real part is 1.85, somewhat larger than the typical values around 1 found in resonance model fits [1]. However, since  $\eta$ -photoproduction is totally s-wave dominated in the first 100 MeV above threshold, the real and imaginary parts cannot be disentangled experimentally.

Fig.4 also shows the calculated cross sections for  $\gamma n \rightarrow \eta n$  together with present (preliminary) extractions from the incoherent  $\eta$ -photoproduction on the deuteron [5]. According to these the  $\eta$ -photoproduction total cross section from the neutron is 2/3 of the proton one with an uncertainty of  $\pm 10\%$ . Our calculation including the anomalous magnetic moment pieces  $\delta \tilde{B}_{0+}^{(2,3)}$  gives a reasonable description of these data. However,

the neutron to proton ratio is not just a constant  $2/3$ , but shows a stronger energy dependence. Finally, in Fig.5 we show the ratio of longitudinal and transverse s-wave multipoles  $|L_{0+}/E_{0+}|$  for  $\eta$ -electroproduction from protons versus the virtual photon momentum transfer  $q^2 < 0$ . The chosen total center of mass energy is  $\sqrt{s} = 1.54$  GeV, where the cross section is expected to be maximal. The ratio has a value of 0.47 at the photon point  $q^2 = 0$  and decreases rapidly, being close to zero at  $q^2 = -0.54$  GeV<sup>2</sup>. In future  $\eta$ -electroproduction experiments at ELSA or CEBAF the longitudinal to transverse ratio  $|L_{0+}/E_{0+}|$  could be measured and it will be interesting to see whether there is indeed a depletion around  $q^2 \simeq -0.5$  GeV<sup>2</sup>.

In Fig.6 we present results for kaon photoproduction,  $\gamma p \rightarrow K^+\Lambda, K^+\Sigma^0, K^0\Sigma^+$ . In these channels the data are more sparse in the region up to 200 MeV above threshold and the statistical weight of these data in our combined fit is therefore low. Nevertheless one finds a good description of the first few data points in each channel. From the measured angular distributions [6,7] only the first data point for  $\gamma p \rightarrow K^0\Sigma^+$  and the first four for  $\gamma p \rightarrow K^+\Lambda$  and  $\gamma p \rightarrow K^+\Sigma^0$  can be considered as s-wave dominated. Interestingly, the  $\gamma p \rightarrow K^+\Lambda$  s-wave total cross section shows a strong cusp at the opening of the  $K\Sigma$ -threshold, which again is a consequence of unitarity and multi-channel dynamics. The present  $\gamma p \rightarrow K^+\Lambda$  data do not clearly show such a cusp and it may be covered by the p-waves which become sizeable above  $E_\gamma = 1.1$  GeV. Interestingly if one divides out of the total cross sections the two-body phase space,  $|E_{0+}(\gamma p \rightarrow K^+\Lambda)|^2$  indeed shows a maximum around  $E_\gamma = 1046$  MeV, the  $K\Sigma$  threshold. Only more data allowing for a multipole decomposition can clarify whether a strong cusp is present in the  $\gamma p \rightarrow K^+\Lambda$  s-wave multipole at the  $K\Sigma$ -threshold. Note that the analogous pion induced reaction  $\pi^- p \rightarrow K^0\Lambda$  (see Fig.7) shows this  $K\Sigma$ -cusp more clearly. The threshold value of the s-wave multipole is  $E_{0+}^{thr}(\gamma p \rightarrow K\Lambda) = (-1.78 - 3.50 i) \cdot 10^{-3} m_\pi^{-1}$  and at the cusp one finds  $E_{0+}^{K\Sigma-thr}(\gamma p \rightarrow K\Lambda) = (-4.06 - 2.36 i) \cdot 10^{-3} m_\pi^{-1}$ . The first two data points for  $\gamma p \rightarrow K^+\Sigma^0$  are somewhat overshoot (see Fig.6) and we find  $E_{0+}^{thr}(\gamma p \rightarrow K^+\Sigma^0) = (4.15 + 3.11 i) \cdot 10^{-3} m_\pi^{-1}$  for the s-wave multipole at threshold, which may be too large in magnitude. One finds however that the first few data points for  $\gamma p \rightarrow K^+\Sigma^0$  do not follow the phase space. Again, more data and a multipole decomposition are needed here. Finally, we show in Fig.6 the  $\gamma p \rightarrow K^0\Sigma^+$  channel. This curve is really a prediction with no data included in the fit and, interestingly, the first data point of the recent analysis [7] is reproduced. The data points further above threshold are not comparable to our s-wave approximation since the measured angular distributions in  $\gamma p \rightarrow K^0\Sigma^+$  are strongly anisotropic. For the threshold value of  $E_{0+}$  we find  $E_{0+}^{thr}(\gamma p \rightarrow K^0\Sigma^+) = (1.34 + 3.38 i) \cdot 10^{-3} m_\pi^{-1}$ . Note that our approach does not have the problem of overpredicting the  $\gamma p \rightarrow K^0\Sigma^+$  channel, at least in s-wave approximation.

### C. Pion Induced Eta and Kaon Production

In Fig.7, we show our results for pion induced eta and kaon production. The cross section data for  $\eta$ -production  $\pi^- p \rightarrow \eta n$  are the selection of [23], and the kaon production cross sections of  $\pi^- p \rightarrow K^0\Lambda, K^0\Sigma^0, K^+\Sigma^-$  and  $\pi^+ p \rightarrow K^+\Sigma^+$  are taken from the compilation [22]. The agreement of the coupled channel calculation with the data is very good even for energies considerably above threshold, except for the (pure isospin 3/2)  $\pi^+ p \rightarrow K^+\Sigma^+$  channel, where the s-wave approximation seems to hold only for the first

data point. Since the pion induced data have quite large error bars their statistical weight is low. Therefore the good agreement with the existing data is a highly non-trivial consistency check of our coupled channel approach which simultaneously describes strong and electromagnetic meson-baryon interactions. As a byproduct of this calculation we extract the  $\eta N$  s-wave scattering length for which we find  $a_{\eta N} = (0.20 + 0.26 i)$  fm. Its imaginary part is almost fixed by unitarity from the rise of the  $\pi^- p \rightarrow \eta n$  cross section and it is in agreement with [24]. However, the real part of  $a_{\eta N}$  is almost a factor of 5 smaller than in the unitary resonance model calculation of [24]. As recently pointed out in [25],  $a_0(980)$ -meson exchange in the t-channel can equally well describe the  $\pi^- \rightarrow \eta n$  total cross sections, but leads to a negative real part of  $a_{\eta N}$ . Therefore we do not consider our small  $\text{Re } a_{\eta N} = 0.20$  fm as unrealistic.

#### D. Nature of the $S_{11}(1535)$ -resonance

The peaks of the observed total cross sections in  $\gamma p \rightarrow \eta p$  (see Fig.4) and  $\pi^- p \rightarrow \eta n$  (see Fig.7) at  $\sqrt{s} \simeq 1.54$  and 1.53 GeV, respectively, suggest the presence of an isospin 1/2 nucleon s-wave resonance, the  $S_{11}(1535)$ . Actually the resonance parameters (mass  $M^*$  and width  $\Gamma$ ) are determined from a fit of the data using a Breit-Wigner parametrization with typical values  $M^* = 1.48 \dots 1.55$  GeV and  $\Gamma \simeq 200$  MeV [1,23]. However the closeness of the  $\eta N$  threshold ( $M_N + m_\eta = 1486$  MeV) causes peculiar features. The  $\eta N$  partial decay width is so strongly energy dependent that the Breit-Wigner curve  $|2(M^* - \sqrt{s}) - i\Gamma(\sqrt{s})|^{-2}$  decreases monotonically from the  $\eta N$  threshold onwards without showing a resonance peak. Furthermore, speed plots (absolute values of derivatives of partial wave amplitudes with respect to  $\sqrt{s}$ ) in [26] derived from  $\pi N$  dispersion analysis show no structure in the  $S_{11}$  partial wave at  $\sqrt{s} \simeq 1535$  MeV, but only the strong  $\eta N$  cusp and the second  $S_{11}(1650)$  resonance. In [27] a calculation of  $\eta$ -production has been performed using the analytically solvable Lee-model and it was found that the data can equally well be reproduced with just a strong background instead of a  $S_{11}(1535)$  resonance pole. The resonance poles actually found in this calculation lie on the wrong (fourth) Riemann-sheet.

Let us now take a closer look at these issues in the present coupled channel calculation based on the chiral Lagrangian. As first pointed out in [15] the chiral  $K\Sigma$  isospin  $I = 1/2$  s-wave interaction is strongly attractive. It can thus built up a resonance-like state with the properties of the  $S_{11}(1535)$ . In Fig.8 we show that eigenphase of the four-channel  $S$ -matrix which below the  $\eta N$ -threshold (marked by an arrow) joins continuously with the elastic  $S_{11} \pi N$  phase. Its value of  $52^\circ$  at the  $\eta N$  threshold is somewhat larger than the empirical  $40^\circ$  (see Fig.2a in [15]). The eigenphase passes through  $90^\circ$  at  $\sqrt{s} = 1584$  MeV with a slope that can be translated into a full width of  $\Gamma = 198$  MeV. These numbers (in particular the one for the width  $\Gamma$ ) are in good agreement with those attributed to the  $S_{11}(1535)$ . However, as one goes up in energy the phase starts to decrease once it has reached  $125^\circ$  at the  $K\Sigma$ -threshold. As required for a clean resonance the phase does not change by  $180^\circ$ . The situation is somehow similar to the isospin  $I = 0$   $\pi\pi$  s-wave at  $\sqrt{s} = 0.88$  GeV where the phase of  $90^\circ$  does not correspond to a scalar resonance but to a strong background.

On the other hand the dynamically generated  $\Lambda(1405)$  in the  $(\bar{K}N, \pi\Sigma)$ -system is a clean resonance in this sense. The  $I = 0$   $\pi\Sigma$  s-wave phase shift, which passes through  $90^\circ$

at  $\sqrt{s} \simeq 1.41$  GeV has moved above  $180^\circ$  at the  $\overline{K}N$  threshold.

Finally, we show in Fig.9 the real and imaginary part of the s-wave multipole  $E_{0+}(\gamma p \rightarrow \eta p)$  in the region  $1.45 \text{ GeV} < \sqrt{s} < 1.67 \text{ GeV}$ . The curves show a resonance-like behavior with the real part of  $E_{0+}$  passing through zero at  $\sqrt{s} = 1545 \text{ MeV}$ . Obviously, in this restricted energy range a clean resonance and a strong background are indistinguishable from each other. We conclude that within our coupled channel approach, the questionable status of the  $S_{11}(1535)$  (resonance or a strong background) is reconfirmed [26,27].

#### IV. SUMMARY

In summary, we have used the SU(3) chiral meson-baryon Lagrangian at next-to-leading order together with a unitary coupled channel approach to describe simultaneously a large number of meson-baryon scattering and meson photoproduction processes. The extension to photo- and electroproduction is parameter free (to order  $q^2$ ). By adjusting only 9 parameters (2 constants in the Lagrangian and 7 finite range parameters) we are able to successfully describe a large amount of low energy data. These include elastic and inelastic  $K^-p$  scattering  $K^-p \rightarrow K^-p, \overline{K}^0n, \pi^0\Lambda, \pi^+\Sigma^-, \pi^0\Sigma^0, \pi^-\Sigma^+$ , eta and kaon photoproduction of protons (and neutrons)  $\gamma p \rightarrow \eta p, K^+\Lambda, K^+\Sigma^0, K^0\Sigma^+$  and  $\gamma n \rightarrow \eta n$  as well as those of the corresponding pion induced reactions  $\pi^-p \rightarrow \eta n, K^0\Lambda, K^0\Sigma^0, K^+\Sigma^-$  and  $\pi^+p \rightarrow K^+\Sigma^+$ . We do not introduce any explicit resonances, but generate the  $\Lambda(1405)$  and  $S_{11}(1535)$  as quasi-bound states of  $\overline{K}N$  and  $K\Sigma$ . We furthermore took a closer look at the nature of the " $S_{11}(1535)$ " in this framework and find that it could well be a strong background instead of a clean resonance. Naturally, the next step for improvement (in particular the description of kaon photoproduction) is the systematic inclusion of the (strong and electromagnetic) p-waves. Given that the s-wave approximation does very well in many channels, this is nontrivial since the p-waves have to be rather selective in the various channels. It remains to be seen whether the p-waves derived from the effective chiral Lagrangian can do this job.

#### Acknowledgements

We are grateful to S. Goers, R. Gothe and B. Krusche for valuable information on the experimental data. We thank S. Goers for providing us with the new  $\gamma p \rightarrow K^0\Sigma^+$  data before publication.

#### Appendix

Here we collect the explicit formulae for the potential coupling strengths  $C_{ij} = C_{ji}$  for the four channel system consisting of the total isospin  $I = 1/2$  meson-baryon states  $|\pi N\rangle^{(1/2)}, |\eta N\rangle^{(1/2)}, |K\Lambda\rangle^{(1/2)}, |K\Sigma\rangle^{(1/2)}$  (labeled by indices 1, 2, 3, 4, respectively) and for the two channel system consisting of the total isospin  $I = 3/2$  states  $|\pi N\rangle^{(3/2)}, |K\Sigma\rangle^{(3/2)}$  (labeled by indices 5 and 6). In this basis one has for the physical states,

$$\begin{aligned} |\pi^- p\rangle &= [\sqrt{2}|\pi N\rangle^{(1/2)} + |\pi N\rangle^{(3/2)}]/\sqrt{3}, \\ |K^+\Sigma^0\rangle &= [|\overline{K}\Sigma\rangle^{(1/2)} + \sqrt{2}|\overline{K}\Sigma\rangle^{(3/2)}]/\sqrt{3}, \\ |K^+\Sigma^-\rangle &= [\sqrt{2}|\overline{K}\Sigma\rangle^{(1/2)} + |\overline{K}\Sigma\rangle^{(3/2)}]/\sqrt{3}, \end{aligned}$$

$$\begin{aligned}
|K^0\Sigma^+\rangle &= [\sqrt{2}|K\Sigma\rangle^{(1/2)} - |K\Sigma\rangle^{(3/2)}]/\sqrt{3}, \\
|K^0\Sigma^0\rangle &= [-|K\Sigma\rangle^{(1/2)} + \sqrt{2}|K\Sigma\rangle^{(3/2)}]/\sqrt{3}.
\end{aligned} \tag{A1}$$

$$\begin{aligned}
C_{11} &= -E_\pi + \frac{1}{2M_0}(m_\pi^2 - E_\pi^2) + 2m_\pi^2(b_D + b_F + 2b_0) - E_\pi^2(d_D + d_F + 2d_0) \\
&\quad + \frac{g_A^2}{4}(3S_{\pi\pi} - U_{\pi\pi}), \\
C_{12} &= 2m_\pi^2(b_D + b_F) - E_\pi E_\eta(d_D + d_F) + \frac{g_A}{4}(3F - D)(S_{\pi\eta} + U_{\pi\eta}), \\
C_{13} &= \frac{3}{8}(E_\pi + E_K) + \frac{3}{16M_0}(E_\pi^2 - m_\pi^2 + E_K^2 - m_K^2) - \frac{1}{2}(m_K^2 + m_\pi^2)(b_D + 3b_F) \\
&\quad + \frac{1}{2}E_\pi E_K(d_D + 3d_F) - \frac{g_A}{4}(3F + D)S_{\pi K} + \frac{D}{2}(D - F)U_{\pi K}, \\
C_{14} &= -\frac{1}{8}(E_\pi + E_K) - \frac{1}{16M_0}(E_\pi^2 - m_\pi^2 + E_K^2 - m_K^2) + \frac{1}{2}(b_F - b_D)(m_\pi^2 + m_K^2) \\
&\quad + \frac{1}{2}E_\pi E_K(d_D - d_F - 2d_1) + \frac{3}{4}(D^2 - F^2)S_{\pi K} + \left(\frac{DF}{2} - \frac{D^2}{6} - F^2\right)U_{\pi K}, \\
C_{22} &= \frac{16}{3}m_K^2(b_D - b_F + b_0) + 2m_\pi^2\left(\frac{5}{3}b_F - b_D - \frac{2}{3}b_0\right) + E_\eta^2(d_F - \frac{5}{3}d_D - 2d_0) \\
&\quad + \frac{1}{12}(3F - D)^2(S_{\eta\eta} + U_{\eta\eta}), \\
C_{23} &= \frac{3}{8}(E_\eta + E_K) + \frac{3}{16M_0}(E_K^2 - m_K^2 + E_\eta^2 - m_\eta^2) + (b_D + 3b_F)\left(\frac{5}{6}m_K^2 - \frac{1}{2}m_\pi^2\right) \\
&\quad - E_\eta E_K\left(\frac{d_F}{2} + \frac{d_D}{6} + d_1\right) + \left(\frac{D^2}{12} - \frac{3}{4}F^2\right)S_{K\eta} + \frac{D}{2}\left(F + \frac{D}{3}\right)U_{K\eta}, \\
C_{24} &= \frac{3}{8}(E_\eta + E_K) + \frac{3}{16M_0}(E_K^2 - m_K^2 + E_\eta^2 - m_\eta^2) + \left(\frac{5}{2}m_K^2 - \frac{3}{2}m_\pi^2\right)(b_F - b_D) \\
&\quad + \frac{1}{2}E_\eta E_K(d_D - d_F) + \frac{1}{4}(3F - D)(D - F)S_{K\eta} + \frac{D}{2}(D - F)U_{K\eta}, \\
C_{33} &= \left(\frac{10}{3}b_D + 4b_0\right)m_K^2 - E_K^2\left(2d_0 + \frac{5d_D}{3}\right) + \frac{3}{4}\left(F + \frac{D}{3}\right)^2 S_{KK} + \frac{3}{4}\left(F - \frac{D}{3}\right)^2 U_{KK}, \\
C_{34} &= 2m_K^2 b_D - E_K^2 d_D + \frac{1}{4}(3F + D)(F - D)S_{KK} + \frac{g_A}{4}(3F - D)U_{KK}, \\
C_{44} &= -E_K - \frac{1}{2M_0}(E_K^2 - m_K^2) + 2m_K^2(b_D - 2b_F + 2b_0) + E_K^2(2d_F - d_D - 2d_0) \\
&\quad + \frac{3}{4}(D - F)^2 S_{KK} - \frac{g_A^2}{4}U_{KK}, \\
C_{55} &= \frac{E_\pi}{2} + \frac{1}{4M_0}(E_\pi^2 - m_\pi^2) + 2m_\pi^2(b_D + b_F + 2b_0) - E_\pi^2(d_D + d_F + 2d_0) + \frac{g_A^2}{2}U_{\pi\pi}, \\
C_{56} &= \frac{1}{4}(E_\pi + E_K) + \frac{1}{8M_0}(E_\pi^2 - m_\pi^2 + E_K^2 - m_K^2) + (m_\pi^2 + m_K^2)(b_D - b_F) \\
&\quad + E_\pi E_K(d_F - d_D - d_1) + \left(\frac{F^2}{2} - DF - \frac{D^2}{6}\right)U_{\pi K}, \\
C_{66} &= \frac{E_K}{2} + \frac{1}{4M_0}(E_K^2 - m_K^2) + 2m_K^2(b_D + b_F + 2b_0) - E_K^2(d_F + d_D + 2d_0) + \frac{g_A^2}{2}U_{KK}.
\end{aligned} \tag{A2}$$

The abbreviations  $S_{\phi\phi'}$  and  $U_{\phi\phi'}$  stand for

$$S_{\phi\phi'} = \frac{E_\phi E_{\phi'}}{2M_0}, \quad U_{\phi\phi'} = \frac{1}{3M_0} \left( 2m_\phi^2 + 2m_{\phi'}^2 + \frac{m_\phi^2 m_{\phi'}^2}{E_\phi E_{\phi'}} - \frac{7}{2} E_\phi E_{\phi'} \right). \quad (\text{A3})$$

The occurrence of  $1/E_\phi$ -terms in  $U_{\phi\phi'}$  reflects the presence of the short cut singularities in the s-wave meson-baryon amplitudes below threshold due to u-channel baryon pole diagrams. Unfortunately, the singularity of the  $1/E_K$ -pole term at  $s = M_\Sigma^2 - m_K^2 > (M_N + m_\pi)^2$  lies slightly above the  $\pi N$  threshold and therefore some (strong and electromagnetic) s-wave potentials become singular at  $\sqrt{s} = 1086$  MeV. In contrast to a proper four dimensional loop integration the used simple Lippmann-Schwinger equation in s-wave approximation is not able to get rid of this singularity in the  $T$ -matrix or  $E_{0+}$ . This feature prohibits a continuation of the present coupled channel calculation down to the  $\pi N$  threshold.

The treatment of meson electroproduction requires the generalization of the  $X_\phi$  and  $Y_\phi$  functions to a transverse and a longitudinal version. There is no change to order  $q^2$  in the  $Y_\phi$  functions, i.e.  $Y_\phi^{\text{trans}} = Y_\phi^{\text{long}} = Y_\phi$ . In contrast to this the  $X_\phi$  functions become more complicated and depend furthermore on the virtual photon momentum transfer  $q^2 = -2t$  as follows:

$$X_\phi^{\text{trans}} = \frac{E_\phi^2 + 3t}{2(E_\phi^2 + 2t)} + \frac{m_\phi^2(E_\phi^2 + 2t) + t^2}{2(E_\phi^2 + 2t)^{3/2}} W_\phi + \frac{E_\phi}{M_0} \left\{ \frac{(m_\phi^2 + 2t)(t - E_\phi^2)}{4(E_\phi^2 + 2t)^2} - \frac{1}{2} + \frac{(m_\phi^2 + 2t)(2m_\phi^2 t - t^2 + m_\phi^2 E_\phi^2 - 2tE_\phi^2)}{4(E_\phi^2 + 2t)^{5/2}} W_\phi \right\}, \quad (\text{A4})$$

$$X_\phi^{\text{long}} = \frac{E_\phi^2}{2(E_\phi^2 + 2t)} + \frac{tE_\phi^2}{2(E_\phi^2 + 2t)^{3/2}} W_\phi + \frac{E_\phi^3}{M_0} \left\{ -\frac{1}{2E_\phi^2} + \frac{(m_\phi^2 + 2t)(4m_\phi^2 t + 3t^2 + 2m_\phi^2 E_\phi^2)}{4(E_\phi^2 + 2t)^2(t^2 + 2tm_\phi^2 + m_\phi^2 E_\phi^2)} + \frac{(m_\phi^2 + 2t)(t - E_\phi^2)}{4(E_\phi^2 + 2t)^{5/2}} W_\phi \right\}, \quad (\text{A5})$$

with the abbreviation

$$W_\phi = \frac{1}{\sqrt{E_\phi^2 - m_\phi^2}} \ln \frac{E_\phi^2 + t + \sqrt{(E_\phi^2 - m_\phi^2)(E_\phi^2 + 2t)}}{\sqrt{m_\phi^2(E_\phi^2 + 2t) + t^2}}. \quad (\text{A6})$$

## Figure Captions

Fig.1 Graphical representation of the Lippmann-Schwinger equation for s-wave meson photoproduction. The full, broken and wavy lines represent baryons, mesons and the photon, respectively.

Fig.2 The total cross sections for the six  $K^-p$  elastic and inelastic scattering channels  $K^-p \rightarrow K^-p, \bar{K}^0 n, \pi^0 \Lambda, \pi^- \Sigma^+, \pi^0 \Sigma^0, \pi^+ \Sigma^-$  versus the kaon lab momentum. The data are taken from [22].

Fig.3 The  $\bar{K}N$  s-wave amplitude with isospin  $I = 0$  versus the total center of mass energy  $\sqrt{s}$ . The dashed and full curve correspond to the real and imaginary part of the scattering amplitude.



- Fig.4 The total cross sections for  $\eta$ -photoproduction off protons and neutrons versus the photon lab energy  $E_\gamma$ . Full circles: MAMI data [1], open squares: ELSA-data [2]. The preliminary neutron data are 2/3 of the proton cross sections with an error bar of  $\pm 10\%$  [5].
- Fig.5 The ratio of longitudinal and transverse s-wave amplitudes  $|L_{0+}/E_{0+}|$  for  $\eta$ -electroproduction off protons at  $\sqrt{s} = 1.54$  GeV versus the virtual photon momentum transfer  $q^2 < 0$ .
- Fig.6 The total cross sections for kaon photoproduction from protons  $\gamma p \rightarrow K^+\Lambda, K^+\Sigma^0, K^0\Sigma^+$  versus the photon lab energy  $E_\gamma$ . The  $K^+$ -data are taken from [6]. The preliminary  $K^0\Sigma^+$  data point has been provided by [7].
- Fig.7 The total cross sections for pion induced eta and kaon production  $\pi^-p \rightarrow \eta n, K^0\Lambda, K^0\Sigma^0, K^+\Sigma^-$  and  $\pi^+p \rightarrow K^+\Sigma^+$  versus the pion lab momentum  $p_{lab}$ . The  $\eta$ -production data are taken from the selection of [23] and the kaon production data from the compilation [22].
- Fig.8 The "resonant" eigenphase of the four-channel S-matrix of the s-wave, isospin  $I = 1/2$  ( $\pi N, \eta N, K\Lambda, K\Sigma$ )-system versus the total center of mass energy  $\sqrt{s}$ .
- Fig.9 Real (dashed line) and imaginary part (full line) of the s-wave electric dipole amplitude  $E_{0+}(\gamma p \rightarrow \eta p)$  versus the total center of mass energy  $\sqrt{s}$ .

## REFERENCES

- [1] B. Krusche *et al.*, *Phys. Rev. Lett.* **74** (1995) 3736.
- [2] B. Schoch, *Prog. Part. Nucl. Phys.* **34** (1995) 43.
- [3] Particle Data Group, *Phys. Rev.* **D50** (1994) 1173.
- [4] B. Krusche *et al.*, *Phys. Lett.* **B358** (1995) 40.
- [5] B. Krusche, Universität Gießen, private communication.
- [6] M. Bockhorst *et al.*, *Z. Phys.* **C63** (1994) 37.
- [7] S. Goers, Universität Bonn, private communication.
- [8] H. Tanabe, M. Kohno and C. Bennhold, *Phys. Rev.* **C39** (1989) 741.
- [9] R.A. Adelseck and B. Saghai, *Phys. Rev.* **C42** (1990) 108; **C45** (1992) 2030.
- [10] L. Tiator, C. Bennhold and S.S. Kamalov, *Nucl. Phys.* **A580** (1994) 455.
- [11] T. Mart, C. Bennhold and C.E. Hyde-Wright, *Phys. Rev.* **C51** (1995) R1074.
- [12] Ch. Sauermann, B.L. Friman and W. Nörenberg, *Phys. Lett.* **B341** (1995) 261.
- [13] Ch. Sauermann, Doktorarbeit, TH Darmstadt (1996).
- [14] N. Kaiser, P.B. Siegel and W. Weise, *Nucl. Phys.* **A594** (1995) 325.
- [15] N. Kaiser, P.B. Siegel and W. Weise, *Phys. Lett.* **B362** (1995) 23.
- [16] For some recent reviews see: G. Ecker, *Prog. Part. Nucl. Phys.* **35** (1995) 1;  
V. Bernard, N. Kaiser and Ulf-G. Meißner, *Int. J. Mod. Phys.* **E4** (1995) 193.
- [17] J. Gasser, H. Leutwyler and M.E. Sainio, *Phys. Lett.* **B253** (1991) 252.
- [18] R. Koch, *Nucl. Phys.* **A448** (1986) 707.
- [19] C. Dover and G. Walker, *Phys. Reports* **89** (1982) 1.
- [20] V. Bernard, N. Kaiser and Ulf-G. Meißner, *Phys. Lett.* **B309** (1993) 421.
- [21] B. Saghai and P.B. Siegel, *Phys. Rev.* **C52** (1995) 392.
- [22] A. Baldini, V. Flaminio, W.G. Moorhead and D.R.O. Morrison, in Landolt-Börnstein, Vol. 12a, ed. H. Schopper (Springer, Berlin, 1988). References to the original data can be traced back from this compilation.
- [23] M. Clajus and B.M.K. Nefkens, in  $\pi N$  Newsletter, **7** (1992) 76.
- [24] M. Batinic, I. Slaus and A. Svarc, *Phys. Rev.* **C52** (1995) 2188.
- [25] B.L. Birbrair and A.B. Gridnev, *Z. Phys.* **A354** (1996) 95.
- [26] G. Höhler, in Proceedings of the International Conference "Physics with GeV Particles", p.198, eds. H. Machner and K. Sistemich, World Scientific, (1995);  
G. Höhler and A. Schulte, in  $\pi N$  Newsletter, **7** (1992) 94
- [27] J. Denschlag, Diplomarbeit, Universität Mainz (1994).

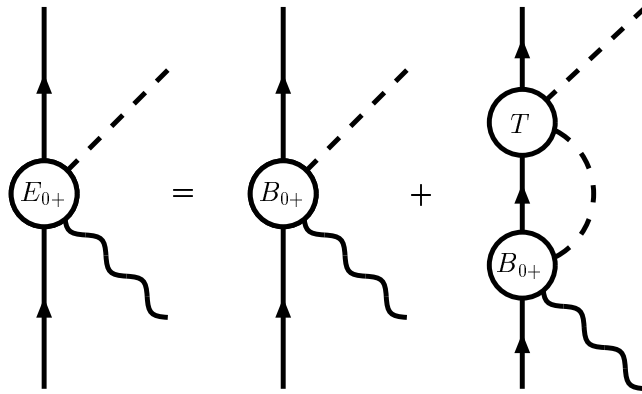


Figure 1

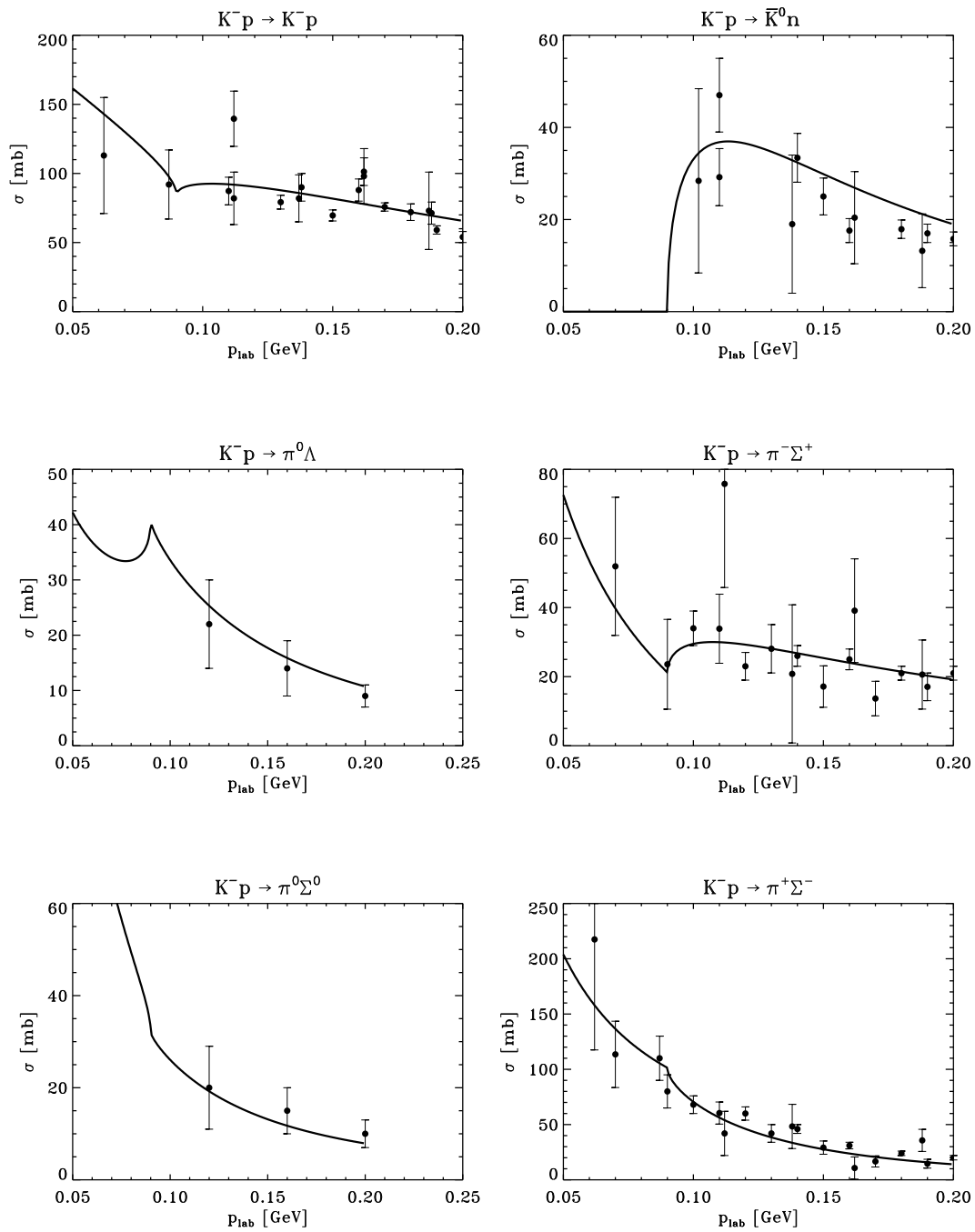


Figure 2

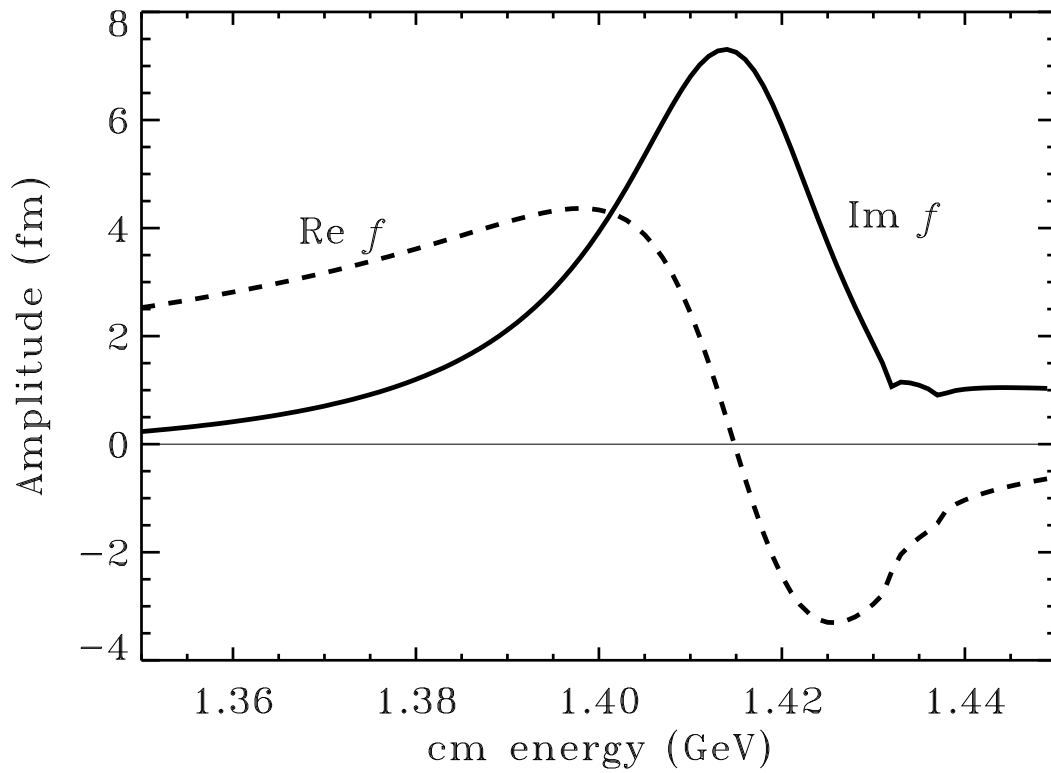


Figure 3

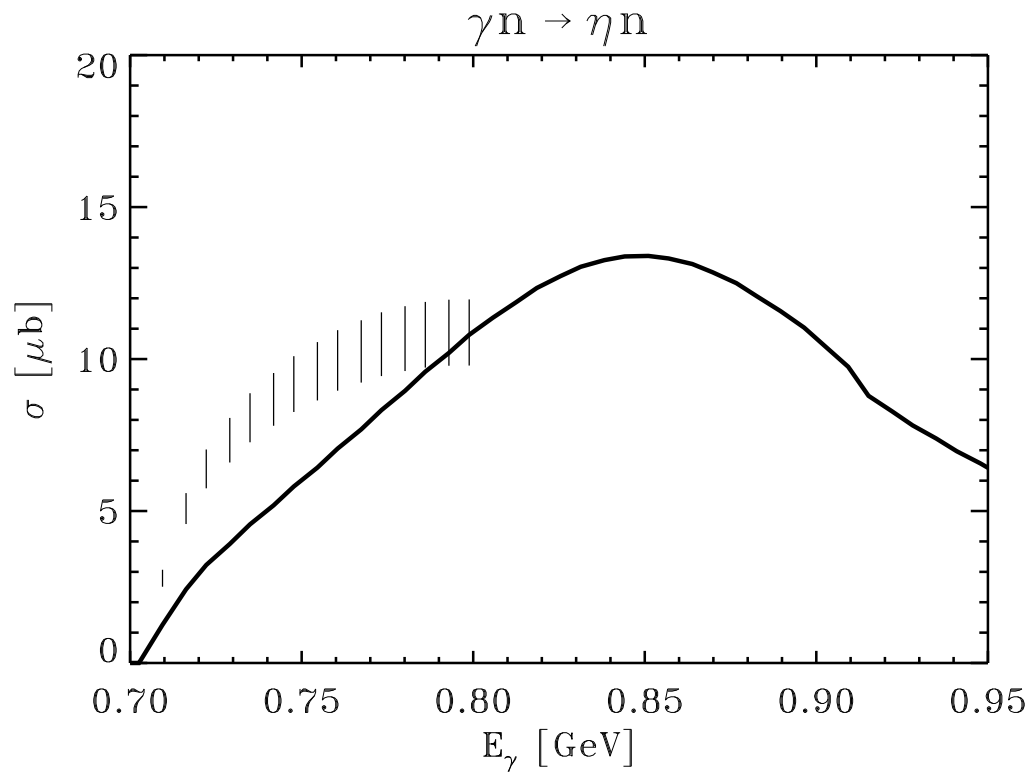
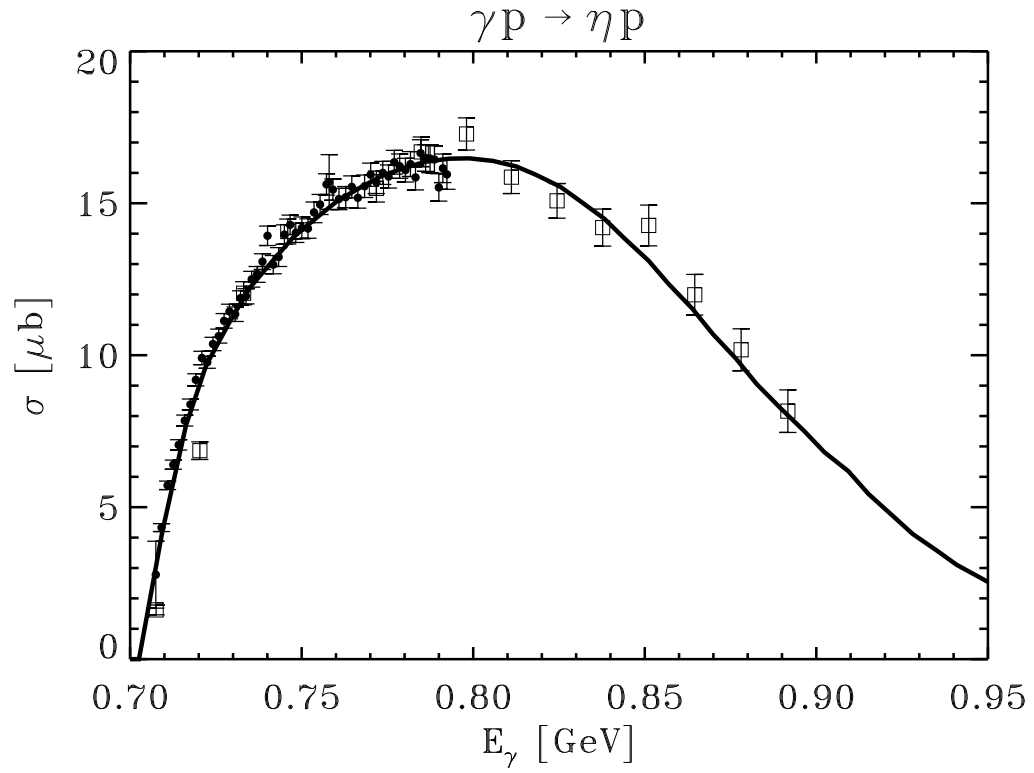


Figure 4

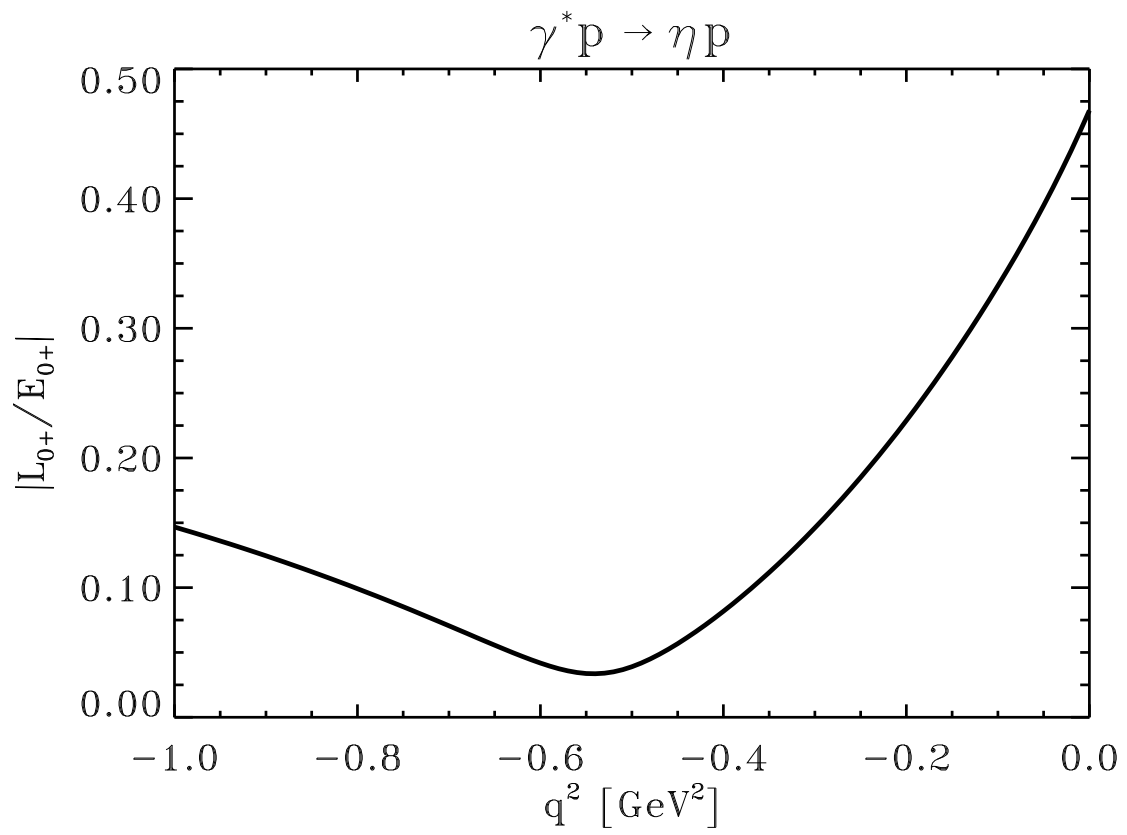


Figure 5

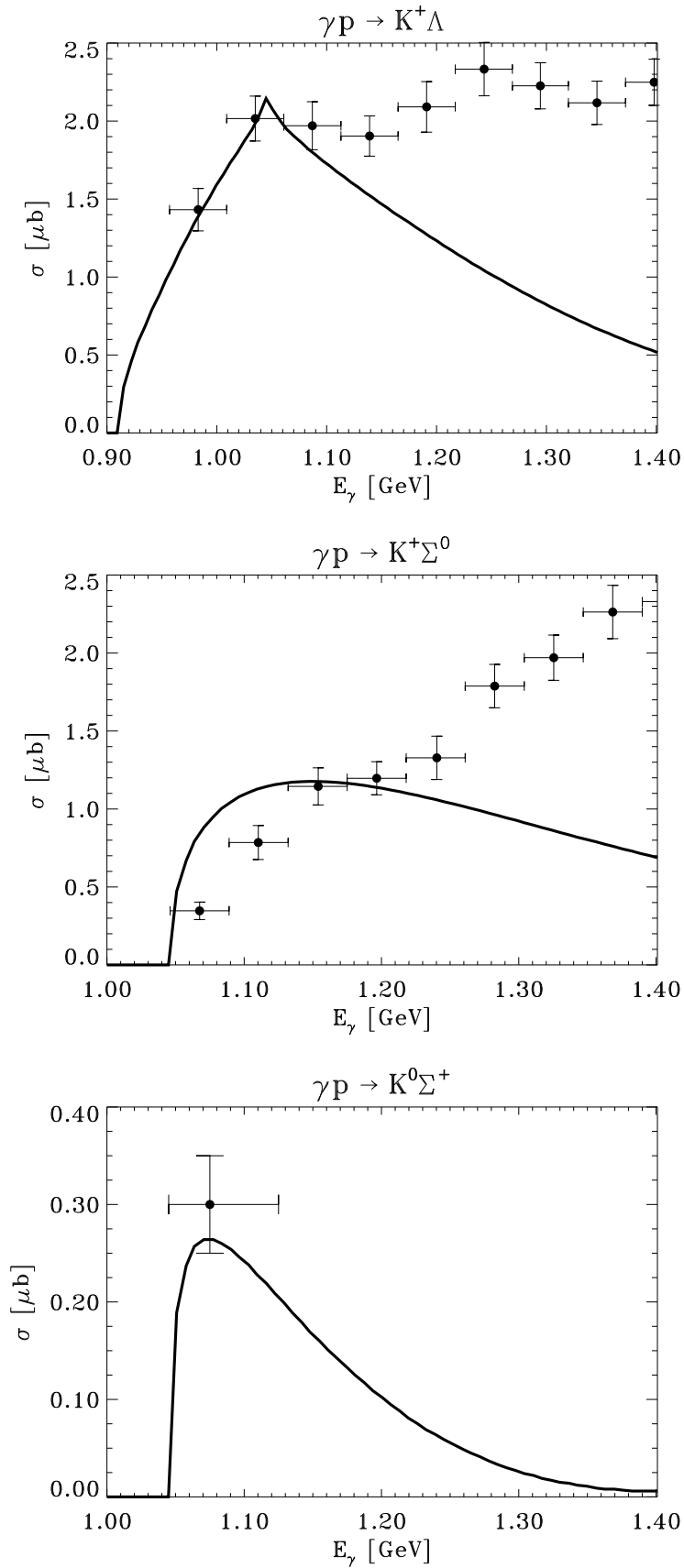


Figure 6



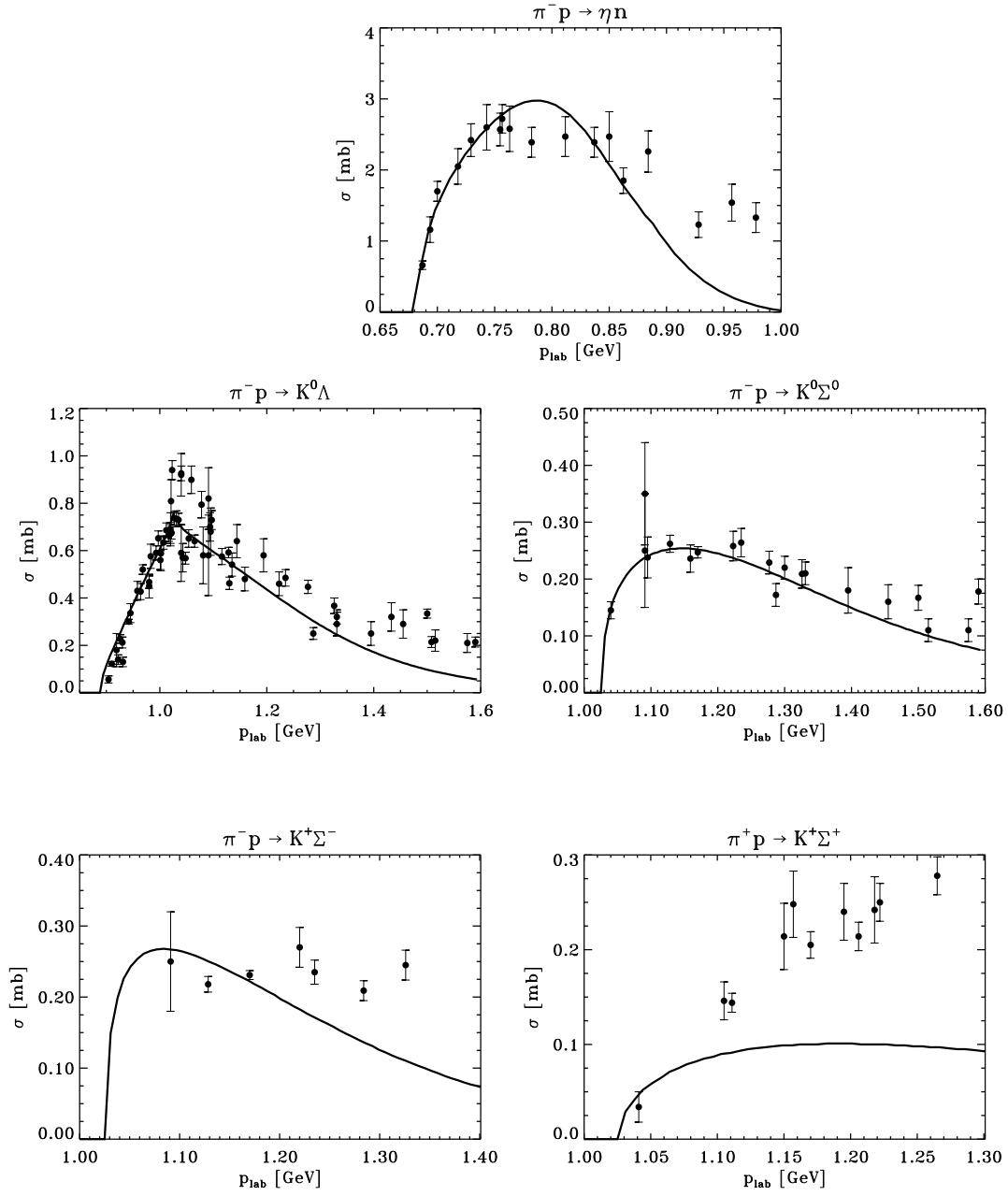


Figure 7

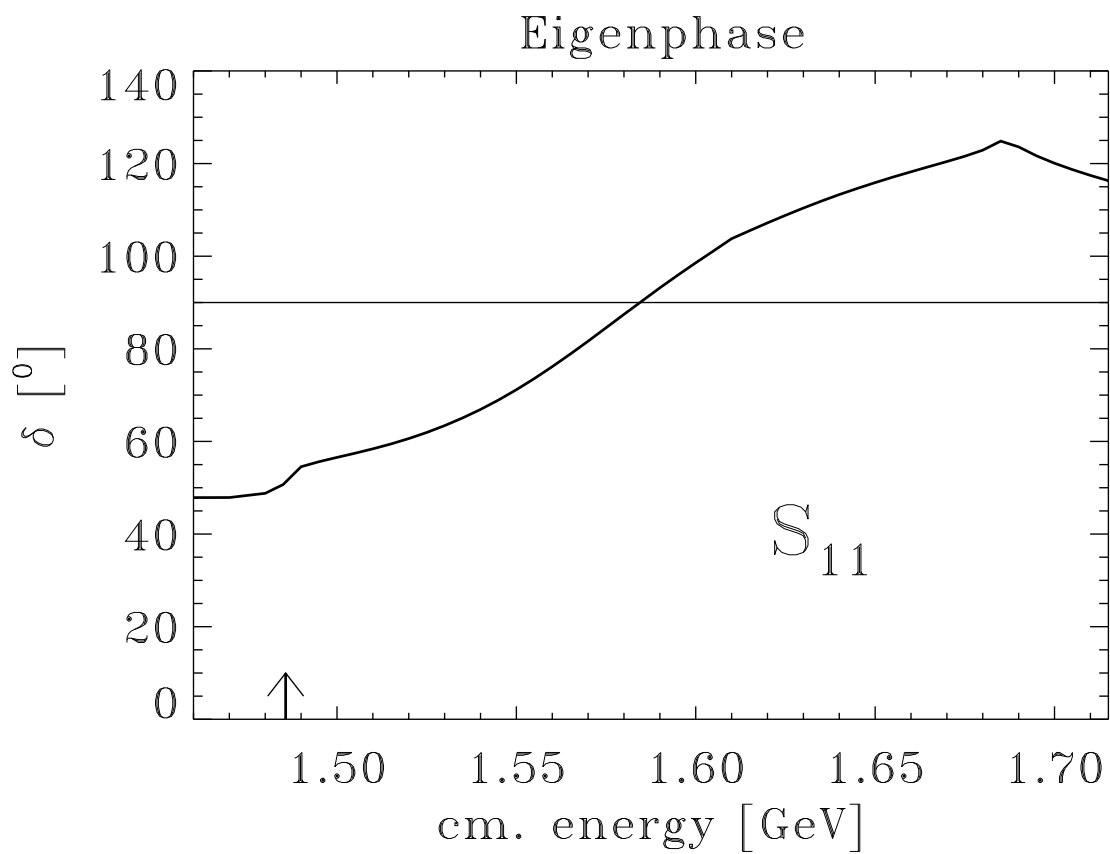


Figure 8

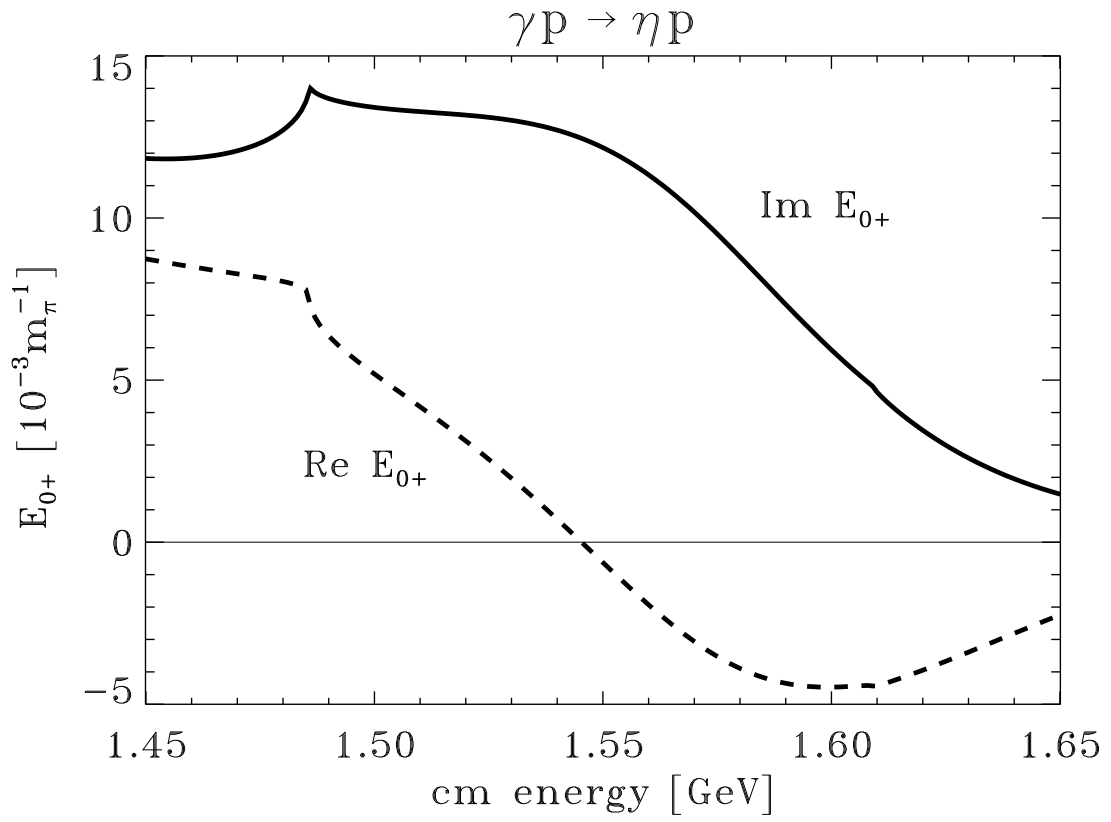


Figure 9